Biophysical Journal Volume 108 February 2015 489–497

Article

Dynamics of Membrane Tethers Reveal Novel Aspects of Cytoskeleton-Membrane Interactions in Axons

Anagha Datar,[1] Thomas Bornschlögl,[2] Patricia Bassereau,[2] Jacques Prost,[2,3] and Pramod A. Pullarkat[1,*]

[1]Soft Condensed Matter group, Raman Research Institute, Bangalore, India; [2]Institut Curie, Centre de Recherche. CNRS, UMR168 Physico-Chimie Curie and Université Pierre et Marie Curie, Paris, France; and [3]Mechanobiology Institute, National University of Singapore, Singapore

ABSTRACT Mechanical properties of cell membranes are known to be significantly influenced by the underlying cortical cytoskeleton. The technique of pulling membrane tethers from cells is one of the most effective ways of studying the membrane mechanics and the membrane-cortex interaction. In this article, we show that axon membranes make an interesting system to explore as they exhibit both free membrane-like behavior where the tether-membrane junction is movable on the surface of the axons (unlike many other cell membranes) as well as cell-like behavior where there are transient and spontaneous eruptions in the tether force that vanish when F-actin is depolymerized. We analyze the passive and spontaneous responses of axonal membrane tethers and propose theoretical models to explain the observed behavior.

INTRODUCTION

In the past few decades there has been a significant advance in the understanding of mechanical properties of bilayer membranes in both synthetic and biological systems. Unlike synthetic membranes, cell membranes are closely associated with the underlying cortical actin that is known to influence mechanical properties of the membranes. For example, in the growth cones of chicken neurons, disruption of F-actin results in a significant reduction in the effective membrane tension and the effective membrane viscosity (1). Another example is the observation that whereas membrane tethers pulled from lipid vesicles can be dragged along the surface of the vesicles (2,3), this phenomenon is not seen in different cells types such as neutrophils (4) and HeLa cells as shown in the present work. This suggests that in cells, the membrane-cortex connection can cause friction at the tether-cell junction and prevent tethers from sliding freely.

Cell membranes stand apart from synthetic lipid membranes in another important aspect. It is known that the steady-state force required for holding a tether pulled from a membrane is directly correlated to the membrane tension. In pure lipid vesicles it has been shown that in the absence of external regulation of membrane tension, the tether force rises with tether elongation (5). However, in the case of cell membranes, this behavior is decided by the rate of tether elongation and probably by the membrane and cytoskeleton organization of the particular cell type (6–9). In fibroblasts, for a range of elongation length the tether force remains constant with respect to tether elongation and the range of tether elongation is a function of the rate of elongation (6). In neuronal growth cones, the tether force dynamically rises with tether elongation but immediately returns to the value corresponding to zero velocity of pulling as soon as the elongation is stopped (7). These facts support the existence of membrane reservoirs that provide the excess membrane required for the tether elongation to maintain the membrane tension at its optimum value in live cells (10). In outer hair cells (8) and *Escherichia coli* (*E. coli*) (9), it has been observed that when tether elongation is stopped, the force relaxes back to the steady-state value over a time of many seconds. However, the exact mechanism of tether force relaxation remains poorly understood.

In the view of the above mentioned aspects, namely, the contribution of cortical cytoskeleton in the dynamics of membrane tethers and the process of tether force relaxation, axonal membranes form an interesting system for the following reasons. First, the static tether force and hence the effective membrane tension value for axonal membrane are significantly lower than that for other cell types (7,11). Second, electron micrographs show that the axonal membrane is smooth and does not contain any detectable folds or membrane structures such as caveolae (12) that can buffer an excess tension. However, it has been proposed that membranous organelles or vesicles could act as a source of extra membrane in axons (13).

The present work aims at understanding the effects of membrane-cytoskeleton interaction on the evolution of axonal tether force. Our results distinguish the scenarios where a multicomponent cell membrane alone can give rise to a characteristic tether force dynamics, from those where the cytoskeleton becomes indispensable. In the first

Submitted June 25, 2014, and accepted for publication November 5, 2014.

*Correspondence: pramod@rri.res.in

Patricia Bassereau, Jacques Prost, and Pramod A. Pullarkat contributed equally to this work.

Editor: Jochen Guck.

0006-3495/15/02/0489/9 $2.00

http://dx.doi.org/10.1016/j.bpj.2014.11.3480

part we study the relaxation of membrane tension after a step-like increase in tether length. We show that the relaxation curve cannot be described by a simple viscoelastic behavior (exponential relaxation). With the help of a model we propose that diffusion of membrane components into the tether across a barrier formed at the tether neck can satisfactorily explain the observations. Next, we study the influence of the actin cytoskeleton in neuronal membrane properties by performing tether sliding experiments along the length of an axon. We see that in contrast with other cell types, membrane tethers pulled from axons can be easily made to slide along the surface of the axon. Based on fluorescent immunolabeling of F-actin, we propose that this behavior is attributable to a sparse and nonuniform distribution of cortical actin in axons. Lastly, we demonstrate occurrence of spontaneous sawtooth-shaped peaks in tether force when the tethers are held unperturbed. The behavior is very similar to that previously reported in tethers pulled from mast cells (14) and in filopodia of HeLa cells (15), where it is proposed to be originating from actin dynamics inside the tether (or filopodium). Although the cause of such spontaneous increase in tether force is unclear in the case of axons, we report that the phenomenon is inhibited in the absence of actin polymerization. This observation suggests that the actin cortex in axons might be sparse but highly dynamic and influences membrane properties in ways previously unexplored.

MATERIALS AND METHODS

Neuronal cell culture

Chicken dorsal root ganglia (DRG) neurons dissected from E7 chicken eggs were seeded after dissociation on untreated, detergent-washed glass cover slips. Cells were grown in L-15 medium (Gibco 11415, Thermo Fischer Scientific, Waltham, Massachusetts) supplemented with NGF-7 (Invitrogen 13290-010, Thermo Fischer Scientific, Waltham, Massachusetts) at the final concentration of 20 ng per mL, 10% Fetal Bovine Serum (Gibco 10100), 33 mM D-glucose (Sigma G6152, Sigma-Aldrich, St. Louis, Missouri), and methyl cellulose 0.6 gm in 100 mL, at 37°C. Many axons were seen to grow up to ~150 μm or longer within 15 h of incubation. Experiments were performed within 15 to 22 h after plating. The medium was changed to the loading medium (everything same as the growth medium except that methyl cellulose is absent) supplemented with a fluorescent dye (FM4-64, Invitrogen, 14 μM) just before the experiment. The sample chamber consisted of two glass cover slips held together using vacuum grease, keeping a gap of ~3 mm in between which was filled with the loading medium and carboxylated polystyrene beads (Spherotech (Lake Forest, Illinois), 1.85 μm in diam., 0.001% suspension). The bottom cover slip had the neuronal cells adhered on its surface. The temperature was maintained at 37°C during the experiment using a microscope objective with a heating collar.

HeLa cell culture

HeLa cells were obtained from the American Type Culture Collection. Cells were grown in RPMI medium (Gibco) containing 10% fetal calf serum (FCS, Gibco) at 37°C in a 5% CO_2 incubator. After rinsing three times in EM buffer, the cells were mounted in a similar microscope chamber as described above with beads (Spherotech, 2.8 μm in diam., 0.001% suspension) and 14 μM FM4-64 dye (Invitrogen).

Drugs

Nocodazole M1404 Sigma (Noco) was used at 20 μM concentration for inhibiting microtubule polymerization. Latrunculin-A L5163 Sigma (Lat-A) was used at 1 μM for inhibiting actin polymerization. Both the drugs were first dissolved in DMSO at high concentration. The final concentration of DMSO in the cell culture medium was less than 0.5%.

F-actin labeling

Neurons were fixed in a solution containing 3.2% paraformaldehyde (Electron Microscopy Sciences 15710, Hatfield, Pennsylvania), 0.05% glutaraldehyde (Electron Microscopy Sciences 16200), PHEM (60 mM PIPES, 25 mM HEPES, 10 mM EGTA, and 2 mM MgCl2, pH 6.9) for 10 min. After rinsing once, the membrane was permeabilized using 0.5% Triton X-100 for 30 min, rinsed and blocked with 5% goat serum for 1 h. After rinsing four times, the cells were incubated in rhodamine-phalloidin (Fluka 77418, Sigma-Aldrich, St. Louis, Missouri) at 25 ng per mL for 20 min at room temperature. After rinsing four times the cells were imaged using Andor iXon885 EMCCD camera (Belfast, United Kingdom).

Force measurement set-up

A custom-built laser trap was used for all the experiments. The set-up consisted of a Ytterbium fiber laser at 1064 nm (IPG Photonics, Oxford, Massachusetts) and a NikonTE2000 confocal microscope (Tokyo, Japan) with a 100×, NA 1.3 oil immersion objective. The sample chamber loaded with cells and beads was tightly clamped onto the microscope stage that was coupled to a voltage-controlled piezo-drive (MadCityLabs). Displacement of a trapped bead from the fixed center of the trap was detected and measured using a quadrant photo diode positioned in the back focal plane of the microscope condenser lens. Trap stiffness calibration was done in situ, just before every experiment using the method described in a previous study (16). The stiffness constant was adjusted around 60 to 65 pN μm^{-1} along X axis and 75 to 80 pN μm^{-1} along Y axis.

Tether experiments

Axons oriented almost parallel to either X or Y axis were chosen for these experiments so that the pulled tether was oriented along X or Y axis, respectively. As the optical trap center itself was fixed in this set-up, all the relative movements were carried out by moving the microscope stage using the piezo-drive. The stage was initially moved so that a selected axon was brought in contact with an optically trapped bead and then moved away from the bead resulting in tether formation. After pulling a tether of length 2 to 5 μm, step-wise displacements of length ~5 μm were applied at a speed ~10 $\mu m\ s^{-1}$.

RESULTS AND DISCUSSION

In all the experiments described in the following sections the observations and measurements were made on preformed tethers of length 2 to 5 μm. For a convenience of notation, the coordinate axes were chosen in such a way that the axon was always oriented along X axis while a tether was oriented along Y axis at equilibrium. Below we present the evolution of tether force after a sudden step-like elongation

of the tether and discuss the possible mechanisms for the observed relaxation.

Force relaxation after step-elongation of a tether

An elongation ΔL of 2 to 5 μm of a preformed tether at the rate of ~10 μm s^{-1} results in a sudden hike in the tether force, which gradually relaxes back to the static force value f_0 as shown in Fig. 1 *A*.

We observed that the tether force relaxes almost back to f_0 even after multiple elongation steps as shown in Fig. 1 *B*, where the tether was elongated by a total of 15 μm. We find for 15 axons, $f_0 = 10.75 \pm 1.87$ pN. These values lie between those reported for growth cones of chicken DRG neurons where $f_0 = 6.6 \pm 0.3$ pN (1) and for mice ganglionic axons where $f_0 = 16 \pm 3$ pN (11). This static force value is a direct measure of the effective membrane tension originating from the in-plane tension on the plasma membrane plus the interaction between the membrane and the cortical cytoskeleton underneath (7). One can estimate the typical axonal membrane tension value by using the following relation:

$$\sigma = \frac{f_0^2}{8\pi^2 B}, \tag{1}$$

where σ is the effective membrane tension, and $B = 2.7 \times 10^{-19}$ N m is the bending modulus of chicken DRG neuronal membrane as measured by Hochmuth et al. (7) used in the rest of this article. Thus we get $\sigma = 5.5 \times 10^{-6}$ N m^{-1}.

Force relaxation behaviors similar to that shown in Fig. 1 have been reported in many different cell types such as outer hair cells (8), *E. coli* (9), and red blood cells (17). However, the single exponential function used in these works does not provide a good fit to the force relaxation data in our experiments on axonal membrane. There has been an attempt in multicomponent synthetic vesicle systems by Campillo et al. at fitting a similar force relaxation behavior to two well-separated relaxation timescales (18). They conjectured that the fast timescale is an effect of the intermonolayer friction (as theoretically formulated in (19)) whereas the slower timescale comes from an unknown diffusive process over the length of the tether. We now discuss different possible relaxation mechanisms and the associated timescales.

The force relaxation behavior can be understood by considering relaxation of a tension gradient along a tubular membrane structure with membrane reservoir(s) at its end(s). It has been shown that the tension equilibration in such a case takes place mainly through two diffusive modes called peristaltic and Lucassen modes (20). The peristaltic mode defines the timescale over which the shape of the tube adjusts to the external conditions, with diffusion constant $D_p = r\sigma/8\eta$ and a characteristic time $\tau_p = \Delta L^2/(4\pi^2 D_p)$ where r is the equilibrium tether radius, ΔL is the wavelength of the mode, and η is the viscosity of the fluid that fills the tube. For a membrane tether, $r = \sqrt{B/2\sigma}$. For our system, r ~0.1 μm and viscosity of the cytoplasm ~10^{-3} Ns m^{-2}, giving D_p ~50 μm^2 s^{-1}. For the longest wavelength mode, ΔL ~5 μm, and the corresponding relaxation time τ_p ~10^{-2} s. Note that the intermonolayer friction, which can play a role in the peristaltic mode, does so at submicron wavelengths. Thus, the corresponding relaxation timescale will be even smaller than 10^{-2} s implying that in the present work, the intermonolayer friction cannot be at play.

The other mode that is called Lucassen mode defines the timescale over which the membrane density (number of lipid molecules per unit area) and the membrane tension reach local mechanical equilibrium by adjusting the membrane crumpling amplitude. It is very fast and controlled by the following diffusion constant:

$$D_\sigma = \frac{Er\left(2\log\left(\frac{L}{r}\right) - 1\right)}{8\eta},$$

with $E = 8\pi B\sigma/(k_B T)$, where E is the entropic stretching modulus of the membrane (21), L is the tether length, η is the fluid viscosity, and σ is the membrane tension. Typical time required for the membrane density to adjust over the whole tether is $\tau_\sigma = \Delta L^2/(4\pi^2 D_\sigma)$. For our experimental system at $T = 37°C$, the order of magnitude estimates are D_σ ~10^5 μm^2 s^{-1} and τ_σ ~10^{-4} s. Considering these significant modes of relaxation, it is clear that in a one-component membrane system, the tether force and the membrane tension would relax much faster than what is observed from

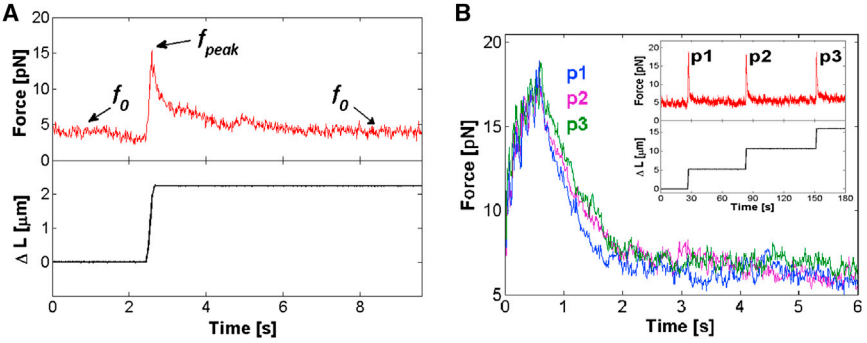

FIGURE 1 (*A*) Evolution of the tether force upon tether elongation. Upper panel shows evolution of tether force with respect to application of a step-like elongation ΔL at speed 10 μm s^{-1} as shown in the lower panel. (*B*) Superposition of tether force evolutions after the three consecutive elongations shown in the inset. Note that at every elongation step, the total tether length is different. The force can be seen to relax to almost the same value after every step. Inset: upper panel shows evolution of tether force with respect to multiple tether elongations by length ΔL as shown in the lower panel.

our experiments (Fig. 1). It may occur that the nanometer size of the tether could give rise to a stronger friction and thus lead to timescales compatible with the experiment. These modes can still be ruled out because they relax in a strongly length-dependent manner, which is not compatible with the data (Fig. 1 *B*).

In a two-component membrane, apart from the peristaltic and the Lucassen modes there exists one more mode of tension relaxation coming from the concentration gradient of the two components. For simplicity, we consider the case where one component has a much smaller surface density than the other. In this limit the tension σ of a membrane composed of a majority constituent with concentration ϕ_1 and minority constituent with concentration ϕ_2 (such that $\phi_1 \gg \phi_2$) has the following form:

$$\sigma = \sigma_1(\phi_1) - \phi_2 k_B T, \tag{2}$$

where the first term is the tension corresponding to the pure majority constituent and the second term is a reduction brought in by the two-dimensional osmotic pressure of the second constituent.

We propose a model for the tether force relaxation mechanism, which is applicable whenever there is a gradient in the membrane composition from the axon to the tether. We make a hypothesis that the neck region at the base of the tether, where there is a sharp change in the membrane curvature, acts as a potential barrier for the ϕ_2 component. Therefore, immediately after tether formation the part of the tether next to the neck region will sense a membrane tension $\sigma = \sigma_1(\phi_1(y_{neck}))$ as $\phi_2 = 0$ because of the neck barrier (see Fig. 2 *A*). The tether is parallel to the *Y* axis as mentioned before, and y_{neck} defines the location of the tether neck. Since the chemical potential for the majority component can quickly equilibrate on both sides of the barrier, $\phi_1(y_{neck})$ is close to its equilibrium value ϕ_1^{eq} in the axonal membrane.

Mechanical equilibrium at constant constituent composition is reached on the timescale corresponding to the peristaltic mode, which is about a few tens of milliseconds.

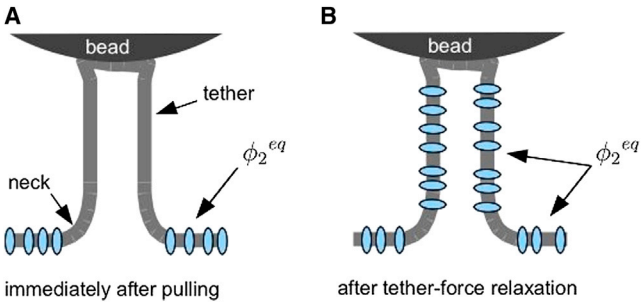

FIGURE 2 A schematic showing the evolution of the density of the minority component ϕ_2 subsequent to tether elongation. (*A*) Immediately after tether formation (or elongation) the concentration ϕ_2 in the tether is below the equilibrium concentration. (*B*) The tether force relaxes as molecules of the minority component cross the barrier and ϕ_2 equilibrates on both sides of the tether neck. To see this figure in color, go online.

This means that the tension adjusts to the value $\sigma_1(\phi_1(y_{neck}))$ all along the tether including the region where $\phi_2 = 0$ as well as in the initially pulled region where $\phi_2 = \phi_2^{eq}$ (when an existing tether is elongated). This is achieved by adapting the membrane crumpling to maintain the total tension homogeneous along the tether. At this point, the tether force is $f = 2\pi\sqrt{2B\sigma_1(\phi_1(y_{neck}))}$. The subsequent force relaxation results from the progressive increase in ϕ_2 as the molecules of the second component cross the barrier at the neck (Fig. 2 *B*). The flux of the second (or minority) component J may be modeled in a simple way by

$$J = \lambda(\phi_2^{eq} - \phi_2(y_{neck})) = -D_m \frac{\partial \phi_2}{\partial y}\bigg|_{y_{neck}},$$

where λ is a dynamic parameter characterizing the barrier, akin to the reciprocal of Kapitza resistance in solid-state physics, and D_m is the diffusion constant of the minority component on the membrane. With the initial condition $\phi_2 = 0$ and Fick's law $\partial\phi_2/\partial t = D_m(\partial^2\phi_2/\partial y^2)$, one obtains $\phi_2(y_{neck}, t) = \phi_2^{eq}\{1 - e^{t/\tau_{cross}}(erfc\sqrt{t/\tau_{cross}})\}$, with a crossover time $\tau_{cross} = D_m/\lambda^2$. This expression is approximate in the sense that it neither takes into account the finite size of the depleted region nor the total tether length. It is valid when the diffusion time τ_m taken for tether length 5 to 10 μm is significantly larger than τ_{cross}. If we assume this to be the case, we obtain the following from Eq. 2:

$$\sigma = \sigma_1(\phi_1^{eq}) - \phi_2^{eq}\left\{1 - e^{t/\tau_{cross}}\left(erfc\sqrt{t/\tau_{cross}}\right)\right\} k_B T.$$

Using this along with Eq. 1 we can write the tether force as the following:

$$f(t) = \sqrt{f_{peak}^2 - \left(f_{peak}^2 - f_0^2\right) g(t/\tau_{cross})}, \tag{3}$$

where the peak force f_{peak} is the tether force immediately after the step-elongation. In this model,

$$f_{peak} = f(t = 0) = 2\pi\sqrt{2B\sigma_1(\phi_1^{eq})}$$

and f_0 as defined earlier, is the force value after stabilization

$$f_0 = f(t = \infty) = 2\pi\sqrt{2B\{\sigma_1(\phi_1^{eq}) - \phi_2^{eq} k_B T\}}$$

and $g(t/\tau_{cross}) = 1 - e^{t/\tau_{cross}}(erfc\sqrt{t/\tau_{cross}})$.

Equation 3 gives a satisfactory fit to the force relaxation curves as shown in Fig. 3 *A*, giving f_{peak}, f_0 and only one timescale τ_{cross}, which is of the order of one-tenth of a second, as the outputs (Table S1 in the Supporting Material). The force can be scaled using the following relation:

$$f_{sc}(t) = \frac{f(t) - f_0}{f_{peak} - f_0} \tag{4}$$

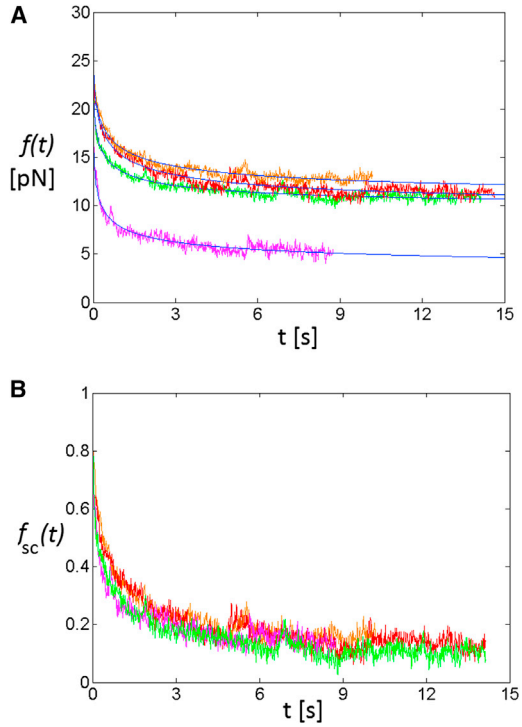

FIGURE 3 (*A*) Relaxation of tether force after a step-elongation applied at $t = 0$. Each color corresponds to a different axon. The corresponding fitting curves obtained using Eq. 3 are shown in blue. (*B*) Rescaled force (Eq. 4) for the four data in (*A*).

so that data from different trials can be seen to overlap (Fig. 3 *B*), indicating that τ_{cross} falls in a narrow range of values for control cells.

The barrier crossing time value $\tau_{cross} = D_m/\lambda^2$ allows us to estimate the amplitude of the potential barrier seen by the diffusing molecules. With $\lambda = (D_m/r)\, e^{\{-(W_b/k_BT)\}}$, where the prefactor is imposed by scaling, the tether radius r ~0.1 μm and D_m ~1 $\mu m^2\, s^{-1}$ (22), we obtain a barrier height W_b of a few times k_BT. Matching the experimentally measured values requires $\phi_2 \sim 5 \times 10^{-15}\ m^{-2}$, i.e., the typical distance between minority molecules to be of the order of 25 to 30 nm. This is a small concentration for nanometer size molecules, justifying our basic approximation. Thus our simple model works surprisingly well. There are many more components in a cell membrane, and it would not be surprising to observe a distribution of the corresponding crossing times. What we see here is clearly the diffusion of the slowest component, which turns out to be well separated from the others.

The connection between membrane and the cortex may have an additional effect on the force relaxation behavior. Our experiments on axons in which F-actin was disrupted using Lat-A show that the relaxation behavior still involves a similar dynamics (Figs. 4 and S1–S4) but the values of the barrier-crossing time τ_{cross} are affected by the cortical integrity (Table S1). Particularly, the crossover time seems to be

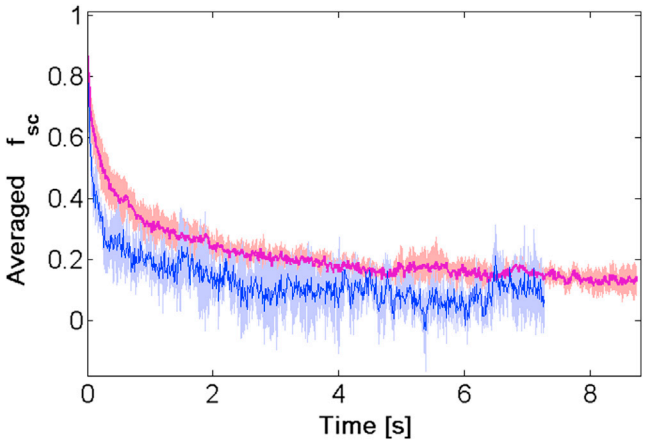

FIGURE 4 Force relaxation after tether step-elongation for control axons (*purple*, averaged over $n = 4$) and Lat-A–treated axons (*blue*, averaged over $n = 3$). Force values are rescaled using Eq. 4. The corresponding shaded regions around each trace show the standard deviation in the data at each time point. Also see additional data in Figs. S1–S4.

smaller for Lat-A–treated axons in comparison with the control axons.

To conclude, the mechanism of tether force relaxation after a step-elongation can be explained purely from gradients formed in the membrane composition. This is consistent with the results obtained from tethers pulled from lipid vesicles with an impurity species in the membrane (18). It is conceivable that if the actin binding proteins present in the membrane contribute to the barrier at the tether neck, the presence/absence of actin can modify the value of the crossover time, without fundamentally changing the form of the force relaxation.

Tether sliding: a way of measuring membrane-cytoskeleton friction

To further explore the effect of membrane-cortex interaction on tether dynamics we next studied the response of tethers to a lateral step-displacement of the axon, resulting in tether sliding on the surface of the axon. The experiments were performed as follows. From an axon oriented along the *X* axis, a tether is pulled along the *Y* axis (Fig. 5 *Ai*) thus the tether force is acting along $+Y$. A step-displacement (at ~10 $\mu m\ s^{-1}$) applied to the sample stage along $+X$, with respect to the optically trapped bead, results in a change in the orientation of the tether with respect to the axon and also results in an elongation of the tether to match the new boundary conditions (Fig. 5 *Aii*). Here, the tether force has both *X* and *Y* components, the former acting in the opposite direction to the applied step-displacement. Thus the tether starts sliding back (Fig. 5 *Aiii*) to regain the perpendicular orientation (Fig. 5 *Aiv*). Fig. 5 *B* shows images of such a tether on an axon, before applying a step-displacement to the stage (i), just after applying the

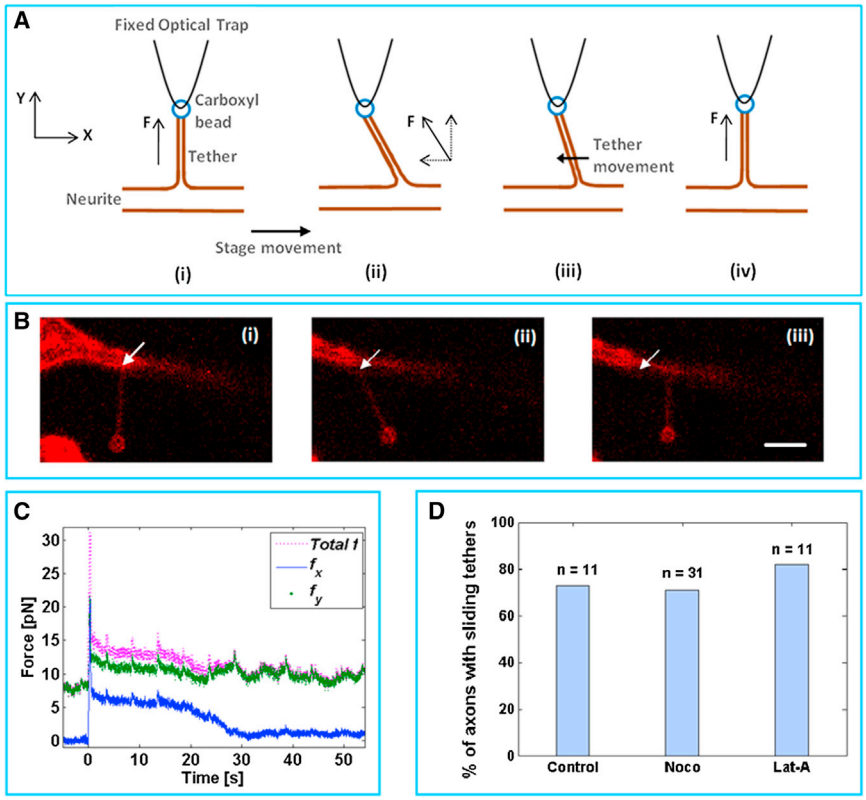

FIGURE 5 (*A*) Depiction of tether step-sliding experiment. (*i*) From an axon oriented parallel to *X* axis a tether is pulled along *Y* axis, hence *X*-component of the tether force $f_x = 0$. (*ii*) The axon is displaced along $+X$ at ~10 μm s^{-1}, resulting in the elongated and slant tether. Thus $f_x \neq 0$ and acts along $-X$. (*iii, iv*) Tether base slides along $-X$ approaching the perpendicular orientation with respect to the axon. (*B*) Confocal images of an axon and a tether (i) just before the step, (*ii*) just after the step, and (*iii*) after the tether base has slid. White arrows point to the initial location of the tether base. Bar = 5 μm. (*C*) Force relaxation after a step-like displacement applied along *X* at $t = 0$. f_x is shown in blue, f_y in green, and the total tether force *f* in pink. Here, the base of the tether is stuck till *t* ~16 s after which it slides till the tether becomes perpendicular to the axon and $f_x = 0$ as in the beginning. (*D*) Comparison of percentage of number of axons on which tether junction is able to slide within the experimental waiting time of 4 to 6 min after applying a step-displacement to Control, Noco-treated, and Lat-A–treated neurons. The population size in each case is n.

step (ii), and after tether sliding (iii). The time lag between application of the step-displacement and the beginning of tether sliding varies over a large range from no observable time lag to a few minutes for different trials. The tether force evolution during one such case is shown in Fig. 5 *C* where a step-displacement was applied to the stage along the long axis of an axon (*X* axis) at $t = 0$. Before this point, the tether was oriented almost along the *Y* axis and therefore $f_x = 0$. The step-displacement initially caused a change in the orientation and a fast elongation along *X* of the tether just as depicted in Fig. 5 *A*, leading to a sharp rise in f_x near $t = 0$. While the tether junction was still stuck, the force relaxed within initial 5 s and stabilized as described in the step-elongation experiments. The tether junction remained stuck until about $t = 16$ s and then began to slide. The subsequent decrease in f_x is because of the tether sliding till the tether was back to its perpendicular orientation with respect to the axon (*t* ~30 s).

When a tether is unable to slide for a time duration longer than the typical waiting duration of 4 to 6 min after the applied displacement and any subsequent displacement of the stage results only in an elongation of the tether, the trial is counted as an unsuccessful sliding trial and vice versa. The percentage of the number of successful trials is plotted as a function of the cytoskeleton drug treatments in Fig. 5 *D*. Each trial is performed on a fresh axon. For comparison, we examined the behavior of tethers pulled from HeLa cells with respect to sliding. The tethers were held at an angle for 5 min. In this condition, one out of five trials resulted in tether sliding in the control cells (Movie S1). When the cells were treated with Lat-A at a concentration greater than 1 μM for more than 1 h, six out of eight trials resulted in tether sliding (Movie S2). Thus, it may be that F-actin in the cortex of HeLa opposes movement of the tether-membrane junction by providing high friction through the membrane-cortex connections. Therefore, it is surprising that even without Lat-A treatment, 70% of the control axons show tether sliding and this percentage is only slightly altered with Noco or Lat-A treatments (Fig. 5 *D*). This is probably attributable to a sparse distribution of F-actin in the cortex of axons or attributable to a weak connection between the actin cortex and the axonal membrane. It is also seen that whether a tether can slide on the axonal surface depends on the location of the tether base. The base may get stuck at a point and take a few minutes before it slides, but it may slide without any delay at some other location. This behavior points toward a heterogeneous cortex. We imaged the F-actin distribution in axons by fluorescent immunolabeling (Fig. 6) that is clearly seen to be inhomogeneous in comparison with microtubule and neurofilament distributions, which are uniform along the length of the axon (Fig. S5). The presence of a periodic distribution of actin filaments has been reported recently in rat hippocampal axons using high-resolution stochastic optical reconstruction microscopy. This structure is said to appear ~5 days onward in vitro (23). We do not see such a

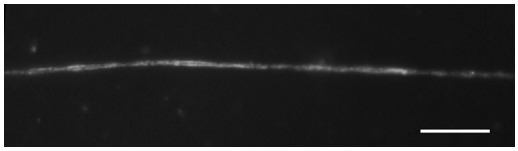

FIGURE 6 F-actin in a fixed and permeabilized axon labeled using Rhodamin-Phalloidin. Bar = 10 μm.

distribution in the chicken embryonic axons studied after 1 day in vitro. Instead we observe a random inhomogeneity as shown in Fig. 6.

During the sliding periods one can estimate the friction coefficient between the base of the tether and the axon. From the data of Fig. 5 *C*, the sliding velocity of the tether base (~0.25 μm s^{-1}) generates a force of the order of a pico-Newton. This corresponds to a friction coefficient μ ~4 $\times$ 10^{-6} N s m^{-1}.

One can identify at least four possible contributions to friction: membrane viscosity, intermonolayer friction because of their differential motion in the neck region, protein detachment/attachment from and to the cytoskeleton, and continuous deformation of the cortex. Considering the friction originating from membrane viscosity only, one expects, ignoring prefactors and log corrections, a friction term of the order of $e.\eta_m$ ~4 $\times$ 10^{-10} N s m^{-1}, where e ~4 nm and η_m ~0.1 N s m^{-2} are the thickness and viscosity of the plasma membrane, respectively (22). This estimate shows that membrane viscosity plays a negligible role in the friction force. Simple scaling arguments suggest that the differential motion of monolayers contribute in a similarly negligible amount to friction.

The contribution of the attachment detachment process between the membrane and the cortex can again be estimated to be of the order of $B\tau n$, where B is the membrane curvature modulus, τ is a typical protein connection time, and n is a surface density of the protein molecules that connect the membrane and the underlying cytoskeleton. Taking a typical value of τ ~ 1 s (24) and taking the bending modulus value of chicken DRG axons from (7) as $B = 2.7 \times 10^{-19}$ N m, one can infer the connecting protein density n necessary to match the experimental value of the friction coefficient μ. The result is more transparent when expressed in terms of the typical distance between connectors, which comes out to be of the order of a few hundred nanometers. This value is similar to the typical value of the F-actin mesh size in the cell cortex (25).

Another contribution to friction comes from the force required to deform the cortex without affecting the protein attachments. It can be estimated to be of the order of $\eta_c f_y^2/E^2 w^3$, where η_c, E, and w are the viscosity, the elastic modulus, and the thickness of the cortex, respectively. With η_c ~ 10^5 Pa s, E ~10^4 Pa (26), and w ~50 nm for axons, one finds the value of the friction coefficient due to cortex deformation to be of the same order of magnitude as the value obtained from the tether sliding experiment. Thus in the regions where the cortex is homogeneous, the last two processes are essentially equivalent. Regions of higher cortical density or with stronger connectors will lead to high friction, thus acting as pinning sites for the lateral movement of a tether.

Apart from these passive responses of the axonal tethers, we also observed F-actin dependent spontaneous changes in the tether force as explained next.

Spontaneous pulling force on tethers

It might be expected that when a tether is held steady, the tether force, once stabilized, stays constant. However, occurrences of sawtooth-like peaks in tether force have been reported in tethers pulled from Mast cells (14). They look qualitatively similar to the load and fail behavior of force exerted by filopodia of HeLa cells (15). We see similar load and fail features in axonal tether force as described below.

In the experiments where the tether force is recorded as a function of time without applying any displacement or perturbation to the system, we see that in ~66% of the trials, the tether force occasionally rises above the static force value till a point after which the force rapidly drops and settles back to the static force value. These events stand apart because of their peculiar slow-rise (over several seconds) and rapid fall (in tens of millisecond) as shown in Figs. 7 *A* and S6. We call them as spontaneous rises or spontaneous peaks of the tether force. The behavior is fundamentally different from the fast-rise and slow-relaxation profile of the tether force in response to tether elongation. The rapid fall is compatible with the fast modes of force relaxation discussed earlier. For the results presented in the earlier sections, only those parts of the force traces devoid of such spontaneous peaks were considered.

We define Δf as the difference between the static force and the peak force just before the sudden drop. It can be seen from Fig. 7 *B* that Δf varies over a wide range of ~2 to 35 pN, and the consecutive peaks are separated by a distribution of time intervals. Often the peak force reaches a value sufficient to pull the bead out of the trap.

Assuming the rise in the tether force during a spontaneous force peak to be linear in time, one can estimate the rate of force build-up (see Table S2), which is of the order of 1 pN s^{-1}. For these measurements we have chosen only the higher peaks with $\Delta f > 8$ pN. This rate of rise in the force is very similar to that observed in filopodia of HeLa cells (15).

Fig. 7 *C* shows that the occurrence of the spontaneous force peaks is highly dependent on the integrity of the axonal cytoskeleton. Here, we have plotted the percentage of trials, which show the spontaneous pulling in control condition and under the action of different cytoskeleton perturbing drugs. It can be seen that whereas Noco reduces the probability of the spontaneous peaks, Lat-A clearly

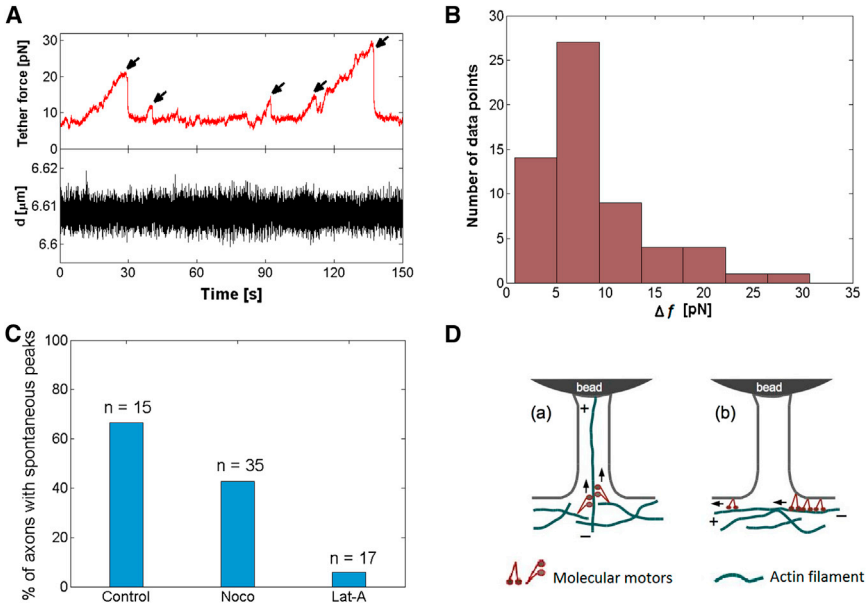

FIGURE 7 (*A*) Spontaneous peaks in the tether force (*upper panel, pointed by black arrows*) while distance *d* between the axon and center of the trap (*lower panel*) is held constant. (*B*) Distribution of Δf for spontaneous force peaks (sample size = 60). (*C*) Percentage of axons showing spontaneous pulling forces. The sample size for each condition is n. (*D*) Proposed models for myosin-driven generation of active force peaks. The arrows indicate the direction of the walking motors. (*a*) Actin filaments grow inside the tether and get attached to the bead. These are pulled by myosin motors present in the cortex. (*b*) Membrane bound motors such as myosin I generate a torque on the membrane as they approach the neck of the tether. Motors moving away from the tether do not contribute to any force. To see this figure in color, go online.

suppresses the phenomenon, suggesting that F-actin is directly involved in the force generation process and microtubules may also play a minor role.

Pinpointing the exact mechanism responsible for these force peaks demands further experiments focusing on the membrane-cytoskeleton interaction. A model based on similar observations of spontaneous force peaks in membrane tethers pulled from mast cells, proposes actin polymerization-depolymerization inside a tether to be at the origin of the force peaks (14). Similar spontaneous features in the force measurement of filopodia of HeLa cells are proposed to be originating from actin filament(s) in the filopodia, which are pulled by the retrograde flow in the cortex (15). Such mechanisms are supported by the observation of actin growing in the membrane tethers (27). We propose that the pulling force may also originate from retrograde movement of actin filaments in the tether because of the action of myosin family motors (see Fig. 7 *D*). Such mechanisms are elaborated in the Supporting Material.

CONCLUSIONS

We have explored various aspects of axonal membrane tension with a particular focus on the role played by the underlying cytoskeleton. We show that the tether force relaxation behavior in response to step-elongation of a tether can be explained by a model where the tether neck forms a potential barrier for a membrane component(s), thus giving rise to a gradient(s) in the membrane composition. This mechanism need not involve the cytoskeleton. Our experiments also reveal hitherto unreported features of axonal membrane, namely, the ability of tether-membrane junction to slide on axonal membrane and spontaneous sawtooth-like peaks in the tether force that are F-actin dependent. Although the former finding suggests that the membrane-cortex linkage is weaker in axons compared with other cell types where tether sliding is not possible, the latter points toward occasional bouts of the cortical activity. Recent high-resolution imaging of axons revealing actin organized as periodically arranged rings (23) highlights the significant structural differences between neuronal cells and other cell types. Further investigations where the cytoskeleton, especially the F-actin is imaged in live axons while the tethers are dragged along the axonal surface or while the spontaneous peaks occur are necessary to understand the mechanisms underlying these features. Photo-bleaching experiments may also shed light on the dynamics of cortical actin that may play a role in some of the effects described above. Such experiments are challenging in the view of small diameter of axons (~0.5 μm) but might be possible with the improving imaging techniques.

SUPPORTING MATERIAL

Supporting Materials and Methods, six figures, two tables, and three movies are available at http://www.biophysj.org/biophysj/supplemental/S0006-3495(14)04744-4.

ACKNOWLEDGMENTS

The authors thank Andrew Callan-Jones and Michel Bornens for illuminating discussions, Roli Srivastava for the help with immunofluorescence labeling, and A. Triller (Ecole Normale Supérieure, Paris) for making provisions to get fertilized chicken eggs for the primary neuron cultures. The tether pulling experiments were conducted at Institut Curie, Paris, where A. D. was supported through the Charpak Fellowship awarded by the Embassy of France in India. P. A. P. acknowledges the Department of Science and Technology, Government of India for support through the Ramanujan Fellowship. T. B. acknowledges the "Human Frontier Science Program" for the funding.

P.B. and J.P.'s groups belong to the Labex CelTisPhyBio (ANR-11-LABX0038) and Paris Sciences et Lettres (ANR-10_IDEX-0001_02).

SUPPORTING CITATIONS

References (28–32) appear in the Supporting Material.

REFERENCES

1. Dai, J., and M. P. Sheetz. 1995. Mechanical properties of neuronal growth cone membranes studied by tether formation with laser optical tweezers. *Biophys. J.* 68:988–996.
2. Evans, E., H. Bowman, …, D. Tirrell. 1996. Biomembrane templates for nanoscale conduits and networks. *Science.* 273:933–935.
3. Cuvelier, D., I. Derényi, …, P. Nassoy. 2005. Coalescence of membrane tethers: experiments, theory, and applications. *Biophys. J.* 88:2714–2726.
4. Liu, B., and J.-Y. Shao. 2012. Tangential tether extraction and spontaneous tether retraction of human neutrophils. *Biophys. J.* 103:2257–2264.
5. Cuvelier, D., N. Chiaruttini, …, P. Nassoy. 2005. Pulling long tubes from firmly adhered vesicles. *Europhys. Lett*. 71:1015–1021.
6. Raucher, D., and M. P. Sheetz. 1999. Characteristics of a membrane reservoir buffering membrane tension. *Biophys. J.* 77:1992–2002.
7. Hochmuth, F. M., J.-Y. Shao, …, M. P. Sheetz. 1996. Deformation and flow of membrane into tethers extracted from neuronal growth cones. *Biophys. J.* 70:358–369.
8. Li, Z., B. Anvari, …, W. E. Brownell. 2002. Membrane tether formation from outer hair cells with optical tweezers. *Biophys. J.* 82:1386–1395.
9. Jauffred, L., T. H. Callisen, and L. B. Oddershede. 2007. Visco-elastic membrane tethers extracted from Escherichia coli by optical tweezers. *Biophys. J.* 93:4068–4075.
10. Gauthier, N. C., T. A. Masters, and M. P. Sheetz. 2012. Mechanical feedback between membrane tension and dynamics. *Trends Cell Biol.* 22:527–535.
11. Pontes, B., Y. Ayala, …, H. M. Nussenzveig. 2013. Membrane elastic properties and cell function. *PLoS ONE.* 8:e67708.
12. Lang, D. M., S. Lommel, …, C. A. O. Stuermer. 1998. Identification of reggie-1 and reggie-2 as plasmamembrane-associated proteins which cocluster with activated GPI-anchored cell adhesion molecules in non-caveolar micropatches in neurons. *J. Neurobiol.* 37:502–523.
13. Dai, J., and M. P. Sheetz. 1995. Axon membrane flows from the growth cone to the cell body. *Cell.* 83:693–701.
14. Farrell, B., F. Qian, …, W. E. Brownell. 2013. Measuring forces at the leading edge: a force assay for cell motility. *Integr Biol (Camb).* 5:204–214.
15. Bornschlögl, T., S. Romero, …, P. Bassereau. 2013. Filopodial retraction force is generated by cortical actin dynamics and controlled by reversible tethering at the tip. *Proc. Natl. Acad. Sci. USA.* 110:18928–18933.
16. Tolić-Nørrelykke, S. F., E. Schäffer, …, H. Flyvbjerg. 2006. Calibration of optical tweezers with positional detection in the back focal plane. *Rev. Sci. Instrum.* 77:103101.
17. Hwang, W. C., and R. E. Waugh. 1997. Energy of dissociation of lipid bilayer from the membrane skeleton of red blood cells. *Biophys. J.* 72:2669–2678.
18. Campillo, C., P. Sens, …, C. Sykes. 2013. Unexpected membrane dynamics unveiled by membrane nanotube extrusion. *Biophys. J.* 104:1248–1256.
19. Evans, E., and A. Yeung. 1994. Hidden dynamics in rapid changes of bilayer shape. *Chem. Phys. Lipids.* 73:39–56.
20. Dommersnes, P. G., O. Orwar, …, J. F. Joanny. 2005. Marangoni transport in lipid nanotubes. *Europhys. Lett.* 70:271–277.
21. Servuss, R. M., W. Harbich, and W. Helfrich. 1976. Measurement of the curvature-elastic modulus of egg lecithin bilayers. *Biochim. Biophys. Acta.* 436:900–903.
22. Domanov, Y. A., S. Aimon, …, P. Bassereau. 2011. Mobility in geometrically confined membranes. *Proc. Natl. Acad. Sci. USA.* 108:12605–12610.
23. Xu, K., G. Zhong, and X. Zhuang. 2013. Actin, spectrin, and associated proteins form a periodic cytoskeletal structure in axons. *Science.* 339:452–456.
24. Evans, E., and K. Kinoshita. 2007. Using force to probe single-molecule receptor–cytoskeletal anchoring beneath the surface of a living cell. *Methods Cell Biol.* 83:373–396.
25. Morone, N., T. Fujiwara, …, A. Kusumi. 2006. Three-dimensional reconstruction of the membrane skeleton at the plasma membrane interface by electron tomography. *J. Cell Biol.* 174:851–862.
26. Pullarkat, P. A., P. A. Fernández, and A. Ott. 2007. Rheological properties of the eukaryotic cell cytoskeleton. *Phys. Rep.* 449:29–53.
27. Pontes, B., N. B. Viana, …, H. M. Nussenzveig. 2011. Cell cytoskeleton and tether extraction. *Biophys. J.* 101:43–52.
28. Smythe, E., and K. R. Ayscough. 2006. Actin regulation in endocytosis. *J. Cell Sci.* 119:4589–4598.
29. Raucher, D., and M. P. Sheetz. 1999. Membrane expansion increases endocytosis rate during mitosis. *J. Cell Biol.* 144:497–506.
30. Bridgman, P. C., and L. L. Elkin. 2000. Axonal myosins. *J. Neurocytol.* 29:831–841.
31. Nambiar, R., R. E. McConnell, and M. J. Tyska. 2009. Control of cell membrane tension by myosin-I. *Proc. Natl. Acad. Sci. USA.* 106:11972–11977.
32. Zot, H. G., S. K. Doberstein, and T. D. Pollard. 1992. Myosin-I moves actin filaments on a phospholipid substrate: implications for membrane targeting. *J. Cell Biol.* 116:367–376.